**PAPER • OPEN ACCESS**

# Error analysis of low-fidelity models for wake steering based on field measurements

View the article online for updates and enhancements.

# Error analysis of low-fidelity models for wake steering based on field measurements

**Stefano Letizia, Paula Doubrawa, Luis A. Martinez-Tossas and Emina Maric**

National Renewable Energy Laboratory (NREL), Golden, CO, United States

E-mail: `stefano.letizia@nrel.gov`

**Abstract.** The observations collected by two scanning lidars deployed on the roof of a 2.8-MW turbine undergoing a series of imposed yaw offsets are analyzed. The wake lateral displacement detected by the rear-facing lidar correlates well with the yaw offset sensed by the forward-facing lidar. We find that the high-frequency part of the yaw offset signal is connected to wake meandering, whereas the low frequency component is a good predictor for wake displacement due to yaw misalignment. Conditionally averaged wake velocity data for different yaw offsets are used as benchmarks for the validation of a linearized Reynolds-averaged Navier-Stokes and an empirical wake model. A mean error as low as 2% and a good prediction of the wake trajectory are achieved, provided that the wake recovery rate matches the observations.

## 1. Introduction

Active wake steering has emerged as one of the most promising wake mitigation strategies and is deemed mature enough to undergo full-scale testing [1]. Pioneering field studies have produced encouraging results [2,3] and inspired numerous theoretical and numerical studies dissecting the origin of wake deflection [4,5], the operation of yawed turbines [6], the influence of the atmospheric state [7] and second-order effects such as secondary steering and yaw direction [8]. The knowledge earned through analytical calculations, high-fidelity simulations and wind tunnel tests has been translated into several reduced-order models for wake deflection [5,9,10,11,12]. Now that the physical mechanisms of wake steering and yaw misalignment have been thoroughly investigated, the next step is to bridge the gap between the idealized framework of the cited studies and real-world scenarios.

Still, a number of pragmatic yet important challenges still prevent the widespread use of wake steering. First, the effect on loads appears less straightforward than the energy counterpart [13]. Second, the main input to this technique, namely the yaw offset, is hardly controllable in real time and is known with high level of uncertainty [14]. Third, wake morphology is governed by atmospheric turbulence that is hard to reproduce in wind tunnels or numerical models [15].

The last problem, which is the focus of this work, has been tackled more recently through the use of nacelle-mounted lidars. For instance, Trujillo et al. [16] observed a delayed onset of wake deflection not predicted by any available model. Fleming et al. [17] report wake deficits whose trajectory agrees fairly well with the predictions by FLORIS, albeit characterized by a markedly different shape. Herges et al. [13] observed a significant wake deflection as a function of the yaw offset and used automated wake tracking to carry out load analysis. Bromm et

al. [18] included several months of hub-height lidar data from near to far wake under neutral conditions to quantify the wake deflection, and showed that the estimated wake trajectory is sensitive to the leveling of the instrument. Brugger et al. [19] adopted a volumetric scanning strategy to quantify wake deflection, which agreed well with low fidelity models. The recent study by Sengers et al. [20] adopted a volumetric reconstruction of mean wake velocity fields that were then used to calibrate an analytical and a data-driven wake model.

This work attempts to shed some light on the different sources of errors of wake models for deflected wake by comparing the simulations to the experimental data collected during the Rotor Aerodynamics, Aeroelastics and Wake (RAAW) project. During RAAW, a 2.8-MW turbine has been heavily instrumented, including the installation of two nacelle-mounted scanning lidars. During an intense observational period of two days, the rotor has been deliberately misaligned and the wake evolution captured, along with essential inflow and turbine performance information. A careful statistical analysis of the lidar data is conducted to build benchmark wake fields that are used to estimate the error of two numerical models.

## 2. Dataset overview

The observations were collected around a 2.8-MW turbine with a rotor diameter $D = 127$ m and a hub height of $H = 120$ m. The top view of the experimental site is given in Fig. 1.
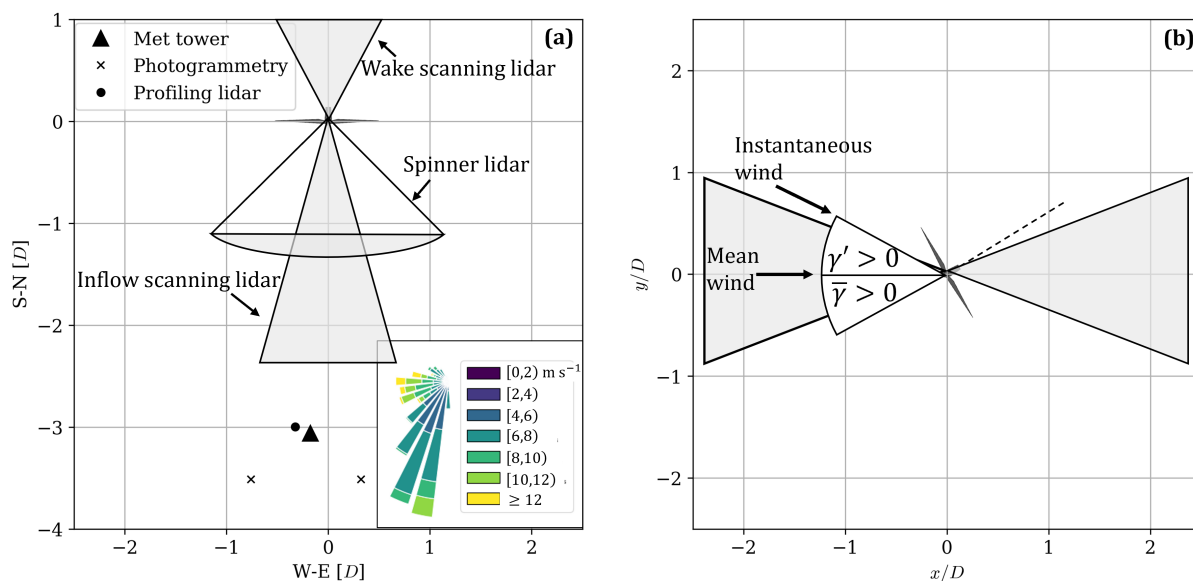


**Figure 1.** Layout of the experimental set up: (a) top overall view of the site in the global reference system and wind rose during the selected period; (b) schematic of the turbine reference system and yaw sign.

The nacelle-mounted inflow and wake scanning lidars represent the object of the current analysis. Both lidars perform a plane position indicator (PPI) scan spanning $\pm 20°$ from the expected wind direction and an angular resolution of $2°$, which takes approximately 20 seconds to complete. The scan is a re-adaptation of the optimal scans for turbulence presented in Letizia et al. [21]. Figure 1b shows a schematic of the lidar scans as well as the yaw conventions.

The yaw offset is achieved by overriding the yaw controller and fixing the rotor at the prescribed offset from wind direction read from the wind vane installed at hub height on the inflow met tower. Yaw offsets from $-30°$ (CW) to $+30°$ (CCW) are held for the duration of 30 minutes with a 0-offset 30-minute buffer interval in between each yaw change. It is convenient to split the total yaw offset seen by the turbine, $\gamma$, into its mean value, $\overline{\gamma}$ based on the mean wind,

and the yaw error, $\gamma\prime$, based on the instantaneous wind. The presence of yaw offset will induce a displacement in the wake for two separate reasons [22]: first, a positive total yaw misalignment, $\gamma$, will induce a transversal force pushing the wake towards negative $y$; second, a positive yaw error, $\gamma\prime$, indicates a negative lateral component that will carry the wake also towards negative $y$. We shall name the first phenomenon a proper "yaw misalignment effect", which would happen also in the absence of yaw error, whereas the second phenomenon is due to advection only and falls more properly within the "wake meandering" category.

The lidar data undergo quality control based on an adaptive signal-to-noise ratio filter. Subsequently, the inflow measurements are leveraged to estimate the real-time incoming wind speed and direction by fitting a cosine function to the radial velocity measurements at the three available upstream distances [23]. The wake observations are used to estimate the instantaneous location of the wake center by fitting a Gaussian function to the de-projected hub-height wind speed [15]. Figure 2 depicts an example of the aforementioned data processing.
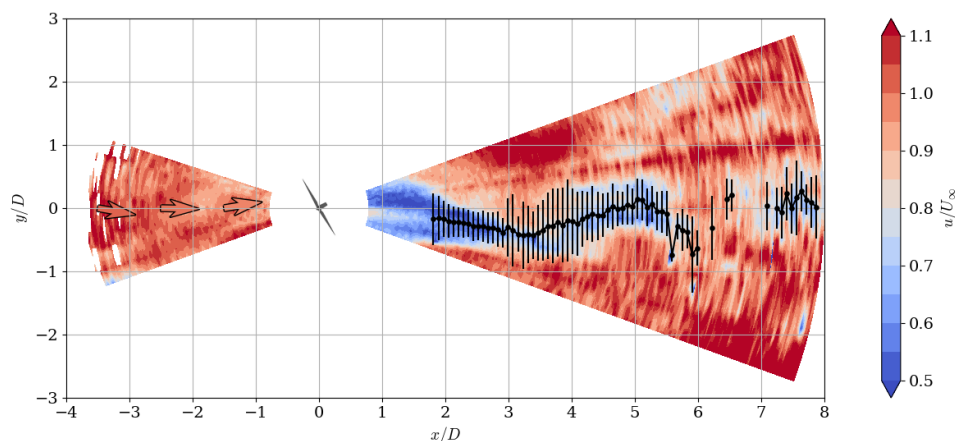


**Figure 2.** Example of processing of instantaneous inflow and wake PPIs.

As a sanity check, the lidar-based inflow is compared to the met tower equivalent at hub height (Fig. 3). All quantities are time-shifted to correct for the streamwise displacement of the different sensors and synchronize them to the wind conditions at the rotor in a Taylor-frozen sense. The advection velocity used for this correction is equal to the 10-minute averaged met tower wind speed. Lidar signals from the three locations shown as arrows in Fig. 2 are averaged together to increase the statistical significance. The best agreement between met tower and lidar is achieved for the wind speed, followed by yaw misalignment and turbulence intensity. The latter is calculated directly as the ratio of lidar wind speed standard deviation to its mean and is then affected by the well-known limitations of the lidar acquisition [24], such as probe/time averaging, noise, and cross-contamination. The lidar-based turbulence intensity is systematically underestimated (likely due to probe/time averaging), although it seems to track well the low-frequency patterns sensed by the met tower. Both lidar and met tower agree that the test periods (which happened during daytime) were characterized by moderate ($5\,\mathrm{m\,s^{-1}}$) to high ($15\,\mathrm{m\,s^{-1}}$) wind speeds and high buoyancy-driven turbulence intensity, except for a period of low turbulence intensity below 10% before 14:00 UTC of day 1. The yaw misalignment time series exhibits significant biases and fluctuations around the target value (green line in Fig 3), which indicates that maintaining a prescribed yaw offset is extremely difficult in a real-world context. The bias is a result of the imperfect alignment of the lidar with the actual mean wind direction and is corrected by realigning the measurements with the 10-minute averaged wind direction during post-processing. The large fluctuations in the lidar-based yaw offset are likely exacerbated by a well-known drawback of nacelle lidars called "cyclops dilemma" [25], namely

the inability to separate the effects of misaligned inflow from horizontal shear in the line-of-sight measurements. Two countermeasures are implemented to mitigate these effects in the inflow lidar data: first, cases with yaw errors larger than the PPI half-opening angle (i.e. 20°) are discarded; second, the remaining yaw error values are scaled by a constant factor of 0.83 to match the standard deviation of the lidar-based observations with that derived from the met tower. The next section will explore the link between the so-obtained yaw offsets and the wake displacement.
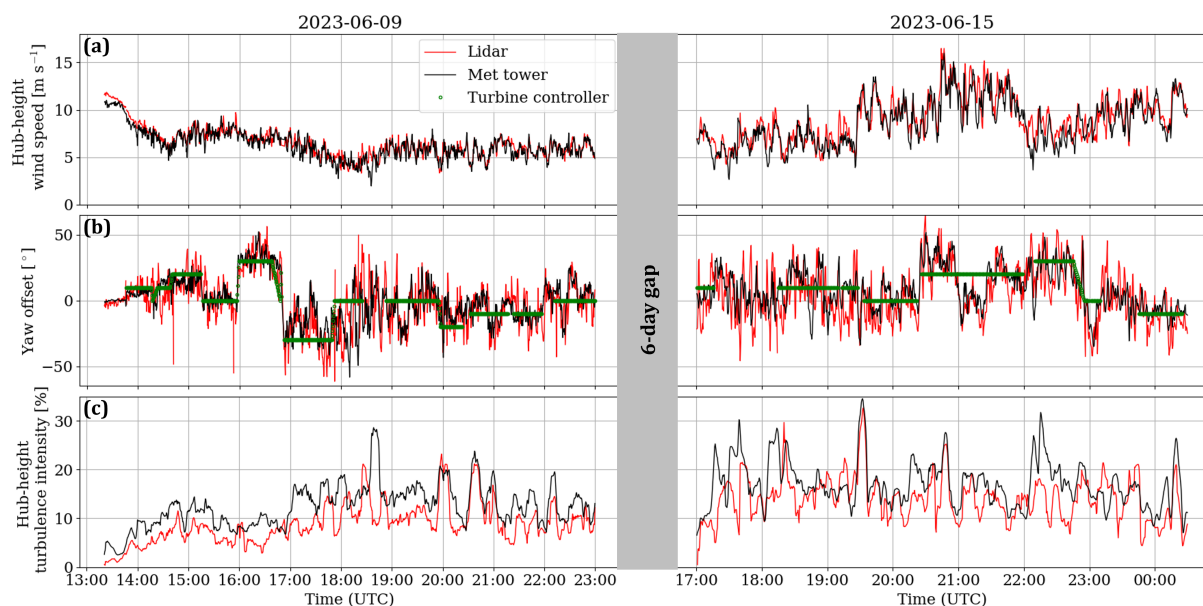


**Figure 3.** Hub-height wind speed, $U_\infty$ (a), yaw misalignment, $\gamma$ (b), and turbulence intensity (c) from met tower and inflow lidar.

## 3. Wake centers analysis

The analysis of the wake center dynamics is aimed at answering two essential questions that are relevant for a well-posed reconstruction of the mean wake velocity field used for model validation:

(i) which sensors provide the best predictor for the yaw misalignment sensed by the turbine?

(ii) how can we disentangle the wake displacement caused by wake meandering from that due to actual yaw misalignment?

To answer the first question, the locations of the wake centers calculated through the Gaussian fit mentioned earlier, $y_c$, are correlated with three predictors of yaw misalignment, $\gamma$. Namely, the yaw offset from the nominal schedule, the met tower and the lidar (green, black and red lines in Fig 3b, respectively) are used as candidates to predict instantaneous wake displacements. Correlation coefficients, $\rho(\gamma, y_c)$, are evaluated for different downstream regions and for different time shifts to test the effect of the advection lag between the rotor (where the yaw offset is defined) and the local wake location. The tested time shifts are converted into shifts in $x$ through the Taylor-frozen hypothesis using tentatively the freestream velocity as a proxy for advection. Based on the aforementioned considerations and the yaw sign convention (Fig. 1b), we anticipate a correlation $\rho(\gamma, y_c) < 0$ between $\gamma$ and $y_c$ as both a positive intentional yaw misalignment and positive yaw error that induces wake meandering should displace the wake towards negative $y$, and vice versa.

Figure 4 shows the correlation coefficients between wake center location and either nominal (Fig. 4a), met-tower-based (Fig. 4b) or lidar-based (Fig. 4c) yaw offset for different downstream
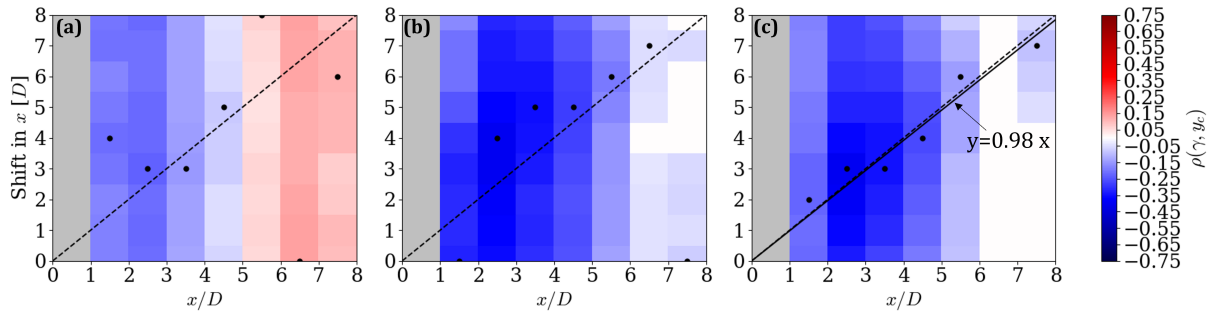
**Figure 4.** Correlation coefficient at different non-overlapping downstream regions and for different shifts in $x$ to account for advection. (a): target yaw offset; (b) yaw offset from met tower; (c) yaw offset from lidar. Values whose 95% confidence interval include 0 are displayed as white. Dots indicate the location of the minimum correlation, the dashed line is the $y = x$ line, and the continuous line in panel (c) is the linear fit of the black dots.

regions (horizontal axis) and advection shifts (vertical axis). Both the yaw based on met tower and lidar predict the expected negative correlation, whereas the nominal yaw offset fails to identify the correct sign of the wake displacement. This substantiates the qualitative observation made around Fig. 3 regarding the challenges of maintaining the desired misalignment in the field experiment. The magnitude of correlations based on both met tower and lidar is similar and decreases moving downstream, suggesting a progressive loss of coherence between the wake displacement in the far wake and the wind conditions at the rotor. The advection shift that provides the best correlation (black dots superposed to the heat map) increases with $x/D$. This means that wake displacements further downstream correlate well with the yaw offset value that occurred further back in time. This is consistent with the hypothesis that the wake deficit acts as a passive tracer "emitted" at the rotor according to the instantaneous thrust and inflow conditions and is advected downstream. The location of the minimum correlation follows closely the expected 1:1 line for the lidar, which is consistent with the expectation of the advection velocity being similar to the freestream value. Based on this finding, all the inflow and yaw information in the remainder of the paper are time-shifted using an advection velocity equal to the freestream value also in the wake region. More importantly, this analysis indicates that the lidar-based yaw misalignment is the predictor of yaw misalignment that better describes the wake center dynamics, thus answering the first of the questions formulated earlier.

To address the second question, namely how the effects yaw misalignment and wake meandering can be separated, it is necessary to predict the effect of meandering that can then be subtracted from the overall wake displacement to single out the contribution of the yaw misalignment. For this purpose, we adopt the well-established Dynamic Wake Meandering (DWM) approach [26]. The wake center prediction by the DWM is implemented as follows:

$$y_{c,\text{DWM}}(x,t) = -\langle U_\infty(t) \sin \gamma(t) \rangle \, \frac{x}{\overline{U}_\infty}, \tag{1}$$

where $-\langle U_\infty(t) \sin \gamma(t) \rangle$ is the time-filtered lateral component of the inflow responsible for the wake meandering and $x/\overline{U}_\infty$ the advection time to location $x$ based on the 10-minute averaged freestream wind speed. The filtering time window for the lateral velocity is chosen according to [19]. The difference between the actual wake center and the DMW estimate is $y_{c,\gamma} = y_c - y_{c,\text{DWM}}$ and according to our hypothesis is due to yaw misalignment only. From a practical standpoint, $y_{c,\gamma}$ will also carry over inaccuracies due to the limits of DWM in reproducing the real-time wake meandering path but we expected these errors to be unbiased and average out when calculating statistics.
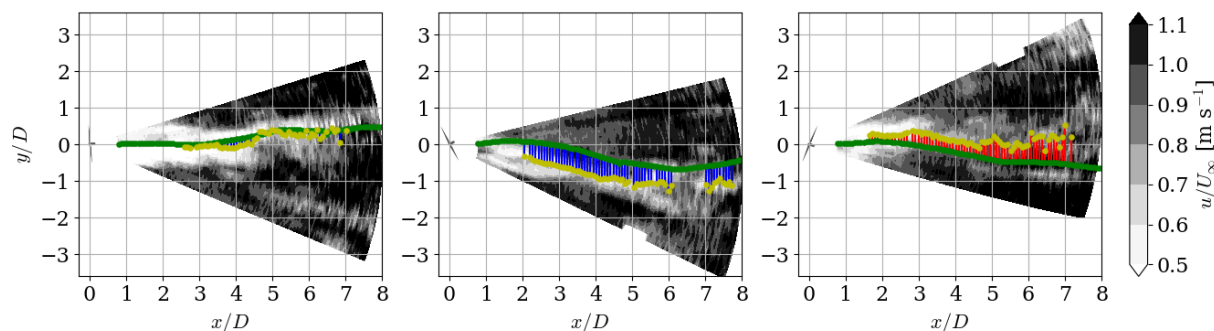
**Figure 5.** Snapshots of wake measurements with the wake center detected through Gaussian fitting, $y_c$ (golden dots), the wake center location predicted by the DWM, $y_{c,\mathrm{DWM}}$ (green dots), and their difference $y_{c,\gamma}$ (red is positive, blue is negative).

Figure 5 illustrates a few snapshots of wake center reconstruction including the DWM prediction for cases with evident wake meandering induced by incoming eddies that are captured by the DWM (green dots). The difference between observed wake center location and DWM output is also highlighted and can be qualitatively correlated to the yaw offset of the turbine. A more quantitative comparison is provided in Fig. 6 where probability density functions and
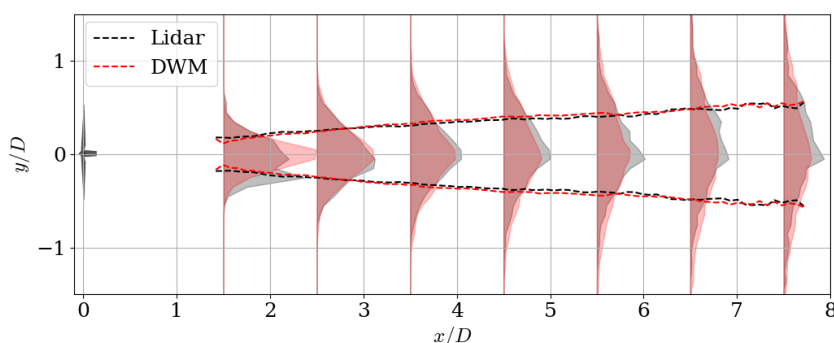


**Figure 6.** Probability density functions of wake centers at different downstream regions (shaded areas) and their standard deviations (dashed lines) from lidar observations (black) and DWM (red).

standard deviations of wake centers are plotted for different non-overlapping downstream regions. The remarkable good agreement of the standard deviations suggests an important conclusion: the dispersion of the instantaneous wake centers is dominated by the meandering component with little additional contribution from yaw misalignment. This implies that for effects of yaw misalignment to emerge it is necessary to average several individual scans with a consistent yaw offset to cancel out the meandering. More pragmatically, there exists a cut-off frequency separating the slow components of yaw offsets signal that will correlate with yaw misalignment, from the fast component that carries information mostly about meandering. To find such a cut-off, we calculate again the correlation between wake centers from lidar, DWM, and their difference and the yaw offset time-filtered but this time with different moving-average windows (Fig. 7).

While the correlation between actual wake centers (Fig. 7a) remains negative for all the averaging window and downstream locations, the one for the wake centers due to meandering only decays fast as the averaging time increases (Fig. 7b). Conversely, the correlation between yaw offset and wake center due to yaw misalignment (Fig. 7c) is initially small or even negative
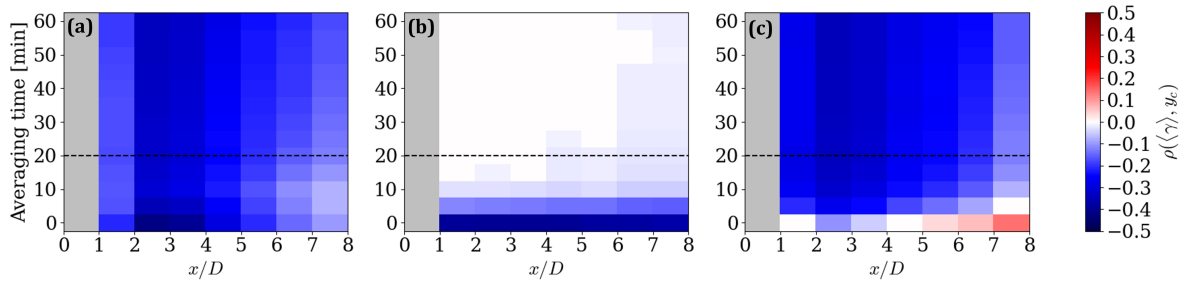
**Figure 7.** Correlation between the time-filtered yaw offset, $\langle\gamma\rangle$ and the wake centers from lidar, $y_c$ (a), DWM $y_{c,\mathrm{DWM}}$ (b) and their difference $y_{c,\gamma}$ (c). The dashed lie is the selected cut-off to separate yaw misalignment from meandering effects.

for a null averaging time and increases as the yaw offset signal is time-filtered more significantly. This analysis reiterates the concept expressed before: fast ($\lesssim 5$ minutes) components of the yaw offset signal trigger essentially wake meandering, while slow ($\gtrsim 5$ minutes) components are more correlated with wake displacement due to yaw misalignment.

Finally, we selected a 20-minute-moving-averaged yaw offset, $\langle\gamma\rangle$, as the best predictor for effects due to yaw misalignment, because it provides the strongest negative correlation with $y_{c,\gamma}$ (Fig. 7c) and is negligibly connected to meandering (Fig. 7b).

## 4. Results

The experimental data are here leveraged to perform error analysis of two wake models, the curled wake model (CWM) [11] and the Gauss-Curl-Hybrid model (GCH) [12]. The first model is a parabolic and linearized Reynolds-averaged Navier-Stokes model with an eddy viscosity turbulence closure. The second, is an empirical Gaussian model that incorporates the curl treatment from the CWM.

In order to maximize the use of the present experimental dataset, benchmark wake velocity fields are built by conditionally averaging lidar velocity data based on the filtered yaw offsets, $\langle\gamma\rangle$. The conditional mean velocity, $\overline{u}$, and turbulence intensity, $I_u$, are calculated through the LiSBOA approach [27] for five bins of yaw offsets identified by inspecting the histogram of $\langle\gamma\rangle$ (Fig. 8). Except for the very first and insufficiently populated cluster (which shows an irregular pattern likely due to poor statistical convergence) the other conditional statistics show meaningful features. The wake is deflected as expected upwards and downwards for negative and positive yaw offsets, respectively, and by a magnitude that appears proportional to the offset. Increased turbulence is also sensed within the deflected wake region. In the following, the mean velocity for clusters 2 to 5 are used as the ground truth for model validation. Boundary and turbine conditions to run the models are approximated as the mean of the respective values for each cluster (Table 1). This approach implicitly assumes that the velocity field varies linearly as a function of the inputs within each cluster and represents an inevitable choice because both wake models are steady. Preliminary analysis of the difference between models and lidars suggested that the wake recovery is a leading factor that can overshadow the effect of wake deflection. To further explore this aspect, simulations are conducted both with a baseline setup and with an optimized turbulence model. The optimization is carried out successfully with a straightforward exhaustive search where values of both the normalized eddy viscosity, $\nu_T$ (made non-dimensional by $U_\infty D$), for the CWM and the wake expansion coefficient, $k_y = k_z$, for the GCH, are varied within allowable ranges (specifically, $\nu_T \in [0.001, 0.02]$ and $k_y = k_z \in [0.01, 0.3]$). Constant values of both $\nu_T$ and $k_y = k_z$ are used for the optimization to eliminate any a priori assumption on their spatial dependence.

The agreement between models and observations is quantified through the Mean Absolute
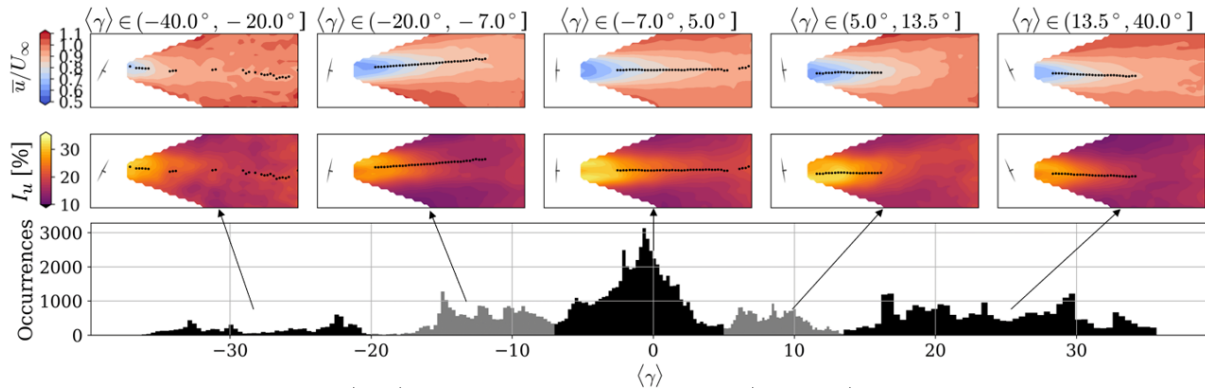
**Figure 8.** Mean velocity (top) and turbulence intensity (bottom) for the five clusters of yaw offset. The histogram of the yaw offset with the bin edges is also provided.

| $\langle\gamma\rangle$ range | $\gamma$ [°] | $U_\infty$ [m s$^{-1}$] | TI [%] | $c_t$ | TSR | Shear exp. | Veer [° m$^{-1}$] |
|---|---|---|---|---|---|---|---|
| $(-20°, -7°]$ | -11.9 | 7.0 | 13.5 | 0.66 | 10.8 | 0.09 | -0.045 |
| $(-7°, 5°]$ | -1.1 | 7.2 | 14.0 | 0.68 | 11.1 | 0.11 | -0.055 |
| $(5°, 13.5°]$ | 8.5 | 6.9 | 13.5 | 0.64 | 11 | 0.25 | -0.005 |
| $(13.5°, 40°]$ | 24.1 | 8.5 | 13.7 | 0.57 | 9.8 | 0.08 | -0.055 |

**Table 1.** Mean inflow and turbine conditions for the selected clusters.

Percentage Error (MAPE), where a 100% error represents a difference equal to the freestream velocity. An overview of the errors is given in Fig. 9. What stands out at a first glance is
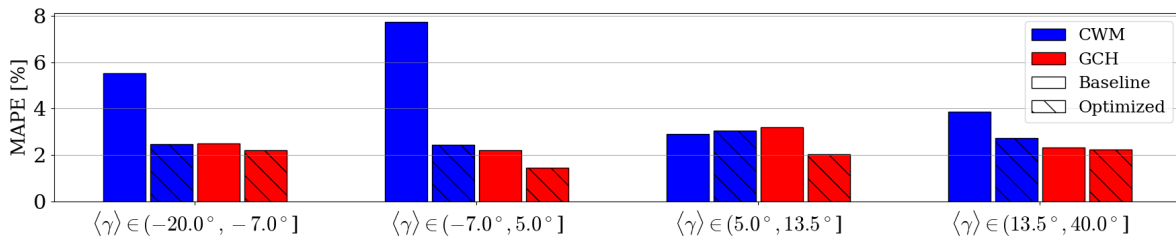


**Figure 9.** Summary of the error between lidar and models.

the large error of CWM with the baseline turbulence model for the first two clusters. A closer look at the velocity fields (Fig. 10) reveals that wake deflection is underestimated by the CWM (continuous line vs. dots) but, most importantly, wake recovers too slowly for the first two cases compared to the experimental data. Those two clusters are also characterized by low shear and high $c_t$ (Table 1). Since the eddy viscosity model in the CWM is essentially driven by shear-generated turbulence, it explains the underestimated wake mixing compared to the real-world buoyancy-driven flow. Optimization of the turbulence model, however, leads to a drastic reduction of the MAPE that drops around 2%, although the wake center trajectory is not improved (not shown). Indeed, optimal values of (constant) eddy viscosity for the CWM model are $\nu_T = 0.006, 0.008, 0.008, 0.004$ for the four clusters, respectively, thus significantly higher than the baseline values shown in Fig. 10.

The baseline GCH performs significantly better than the CWM thanks to the empirical wake expansion coefficient that is related to the ambient TI, thus including also the influence of thermal convection. Optimizing the turbulence model improves the agreement with lidar data just marginally, although the values of the optimal wake expansion coefficients (Fig. 11) are higher than their baseline counterparts ($k_y = k_z = 0.055, 0.057, 0.055, 0.056$). Velocity fields for the optimized GCH, which is the best-performing model, are shown in Fig. 11. The wake center
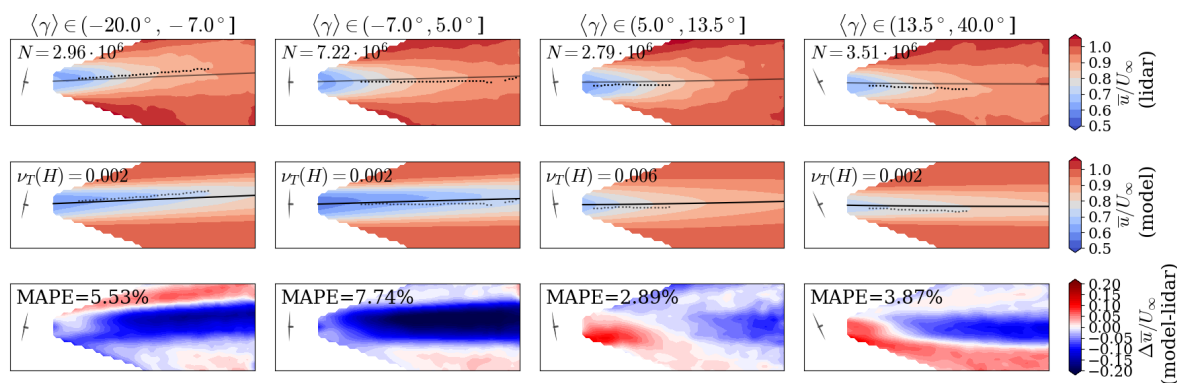
**Figure 10.** Mean velocity from clustered lidar data (top), CWM with baseline turbulence model (middle) and their difference (bottom). Dots and continuous line are the wake centers of the lidar and simulations, respectively.

trajectory, which was minimally changed from the baseline, agrees well with the observations, except for the far wake of the first cluster, possibly due to non-linear effects occurring within the cluster itself. The error distribution highlights that most of the discrepancy occurs in the near wake and due to a different shape of the initial velocity deficit, with the GCH having a narrower/deeper profile than the lidar. However, this aspect is of secondary importance for real applications because wake interactions occurs generally at distances greater than 3 diameters.
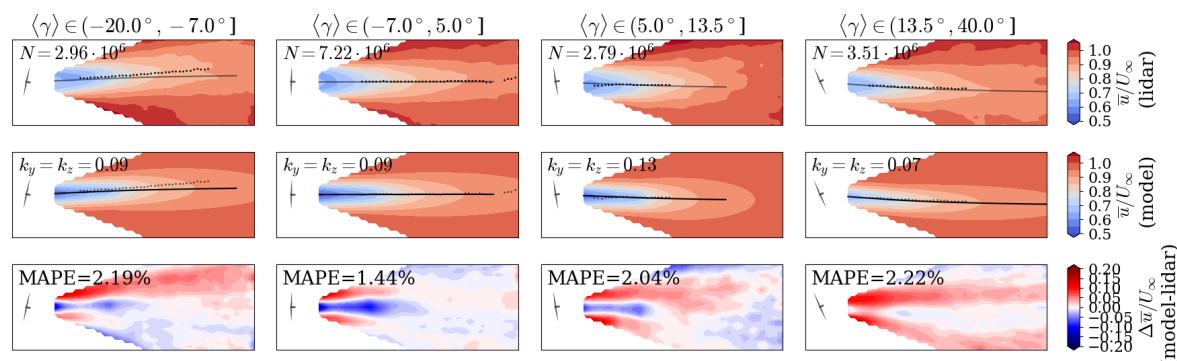


**Figure 11.** Like Fig. 10 but for optimized GCH.

## 5. Conclusions

Experimental data collected by a forward-facing and a rear-facing scanning lidars have been used to build conditionally-averaged statistics of wake velocity under different yaw offsets and used for model validation. The main challenge from the experimental standpoint was the identification of the best predictor of yaw misalignment effects on wake deflection, which turned out to be the 20-minute averaged yaw offset from the inflow lidar. This parameter is representative of the wind state at the turbine and varies sufficiently slow to allow wake meandering effects to cancel out. Cluster statistics as a function of yaw offset reveal a wake deflection that agrees in sign with theoretical models. The result is significant mainly because it is obtained for a relatively short campaigns (2 days) compared with similar studies [18,19] that took several weeks. The CWM and GCH were able to capture the relevant physics in terms of yaw deflections and their initial errors before tuning the turbulence effects are below 10% of the freestream velocity. However, the CWM and GCH performed differently when compared to the observations. The first one

in its baseline version tends to under-predict the wake recovery but significantly improves after tuning the eddy viscosity to account for buoyancy-driven turbulence. The second one has a 2% error in its baseline version, which is driven by differences in the near-wake shape and improves minimally when recalibrating the wake expansion coefficient. The GCH also has a better agreement with experimental data for the wake deflection. This analysis highlights two possible improvements for models: for the CWM, an enhanced turbulence model suitable for non-neutral stability conditions; for the GCH, an adaptable thrust distribution to match specific turbine models.

## Acknowledgments

## References

[1] Houck D 2021 *Wind Energ.* 1-25
[2] Fleming P *et al* 2017 *Wind Energ. Sci.* **2(1)** 229–39
[3] Howland M F, Lele S K and Dabiri J O 2019 *Proc. Nat. Acad. Sci. USA* **116(29)** 14495–500
[4] Shapiro C R, Gayme D F and Meneveau C 2018 *J. Fluid Mech.* **841** R11-R112
[5] Bastankhah M and Porté-Agel F 2016 *J. Fluid Mech.* **806** 506–41
[6] Howland M F *et al* 2020 *J. Renew. Sustain. Energ.* **12** 063307
[7] Vollmer L, Steinfeld G, Heinemann D and Kühn M 2016 *Wind Energ. Sci.* **1(2)** 129–141
[8] Fleming P *et al* 2018 *Wind Energ. Sci.* **3(1)** 243–55
[9] Jimenez A, Crespo A, Migoya E 2010 *Wind Energy* **13** 559-7-2
[10] Qian, GWa and Ishihara, T 2018 *Energies* **11(665)**
[11] Martinez-Tossas L A, Annoni J, Fleming P A, and Churchfield M J 2019 *Wind Energ. Sci.* **6(3)** 701–14
[12] King, J, Fleming P, King R, Martínez-Tossas L A, Bay C J, Mudafort R and Simley E 2021 *Wind Energ. Sci.* **4(1)**
[13] Herges T G, Berg J C, Bryant J T, White J R, Paquette J A and Naughton B T 2018 *J. Phys.: Conf. Ser.* **1037(7)**
[14] Simley E, Fleming P, King J 2020 *Wind Energ. Sci.* **5(2)** 451–68
[15] Zhan L, Letizia S and Iungo G V 2019. *Wind Energ.* **23(3)** 501–27
[16] Trujillo J J, Schlipf D, Würth I, Seifert J K and Kühn M 2016 *Wind Energ. Sci.* **1** 41–53
[17] Fleming P *et al* 2017 *J. Phys.: Conf. Ser.* **854** 012013
[18] Bromm M, Rott A, Beck H, Vollmer L, Steinfeld G and Kühn M 2020 *Wind Energ.* **21(11)** 1011–28
[19] Brugger P, Debnath M, Scholbrock A et al. 2020 *Wind Energ. Sci.* **4(5)** 1253–72
[20] Sengers B A M, Steinfeld G, Hulsman P and Kühn M 2023 *Wind Energ. Sci.* **8(5)** 747–70
[21] Letizia S et al. 2023 *J. Phys.: Conf. Ser.* **2505** 012048
[22] Abraham A, Martinez-Tossas L A and Hong J 2021 *J. Fluid. Mech.* **926** A29-1
[23] Carbajo Fuertes F, Markfort C D and Porté-agel F 2018 *Remote Sens.* **10** 668
[24] Penã A, Mann J and Dimitrov N 2017 *Wind Energy Sci.* **2(1)** 133–52
[25] Letizia S *et al* 2023 *Frontiers Mech. Eng.* **9** 1261017
[26] Larsen G, Madsen, H A, Thomsen, K and Larsen, T J 2008 *Wind Energy* **11(4)** 377–95
[27] Letizia S, Zhan L and Iungo G V 2021 *Atmos. Meas. Tech.* **14** 2065–93